ISBN: 978-3-95450-223-3 ISSN: 2673-7000 doi:10.18429/JACoW-NAPAC2019-MOPLM14

STUDIES OF BEAM DUMPS IN CANDIDATE HORIZONTAL COLLIMATOR MATERIALS FOR THE ADVANCED PHOTON SOURCE UPGRADE STORAGE RING*

J. Dooling†, W. Berg, M. Borland, G. Decker, L. Emery, K. Harkay, R. Lindberg, A. Lumpkin, G. Navrotski, V. Sajaev, Y-P. Sun, K. P. Wootton, A. Xiao
Argonne National Laboratory, Lemont, IL, USA

Abstract

We present the results of experiments on the effects of beam dumps on candidate collimator materials for the Advanced Photon Source Upgrade (APS-U) storage ring (SR). Due to small transverse electron beam sizes, whole beam loss events are expected to yield dose levels in excess of 10 MGy in beam-facing components, resulting in localized melting. Whole beam aborts have characteristic time scales ranging from 100s of ps to 10s of microseconds which are either much shorter than or roughly equal to thermal diffusion times. Aluminum and titanium alloy test pieces are each exposed to a series of beam aborts of varying fill pattern and charge. Simulations suggest the high energy/power densities are likely to lead to damage in any material initially encountered by the beam. We describe measurements used to characterize the beam aborts as well as results of post-experiment inspection. The goal of this work is to guide the design of APS-U SR collimators. Simulations are discussed in a companion paper at this conference.

INTRODUCTION

The Advanced Photon Source (APS) is building a fourth-generation storage ring to replace the present double-bend achromat lattice with a multibend achromat [1], allowing generation of ultra-bright x-ray beams. The APS upgrade (APS-U) [2] will be able to produce these ultra-bright beams because of a 100-fold reduction in horizontal emittance and a two-fold increase in current. The APS-U electron beam has such high energy and power densities that virtually any material the beam strikes will be damaged [3].

We have previously seen damage from beam strikes in high-Z, high-density materials such as copper and tungsten use to fabricate vertical and horizontal scrapers at various locations at APS [4]. Two promising materials for the APS-U horizontal, whole-beam-dumps are aluminum alloy 6061-T6 (Al) and titanium alloy Ti-6Al-4V (Ti6Al4V or TiA); the former for its high thermal diffusivity and low Z, the latter for its strength and high melting temperature. Two collimator test pieces, one from each alloy, were fabricated and used during this study. Photographs of the copper scraper body with the Al and TiA test pieces are presented in Fig. 1 prior to testing with beam. The scraper is shown fully extended into the vacuum chamber, with the Al collimator on top. A 1-mm vertical gap exists between the test pieces.

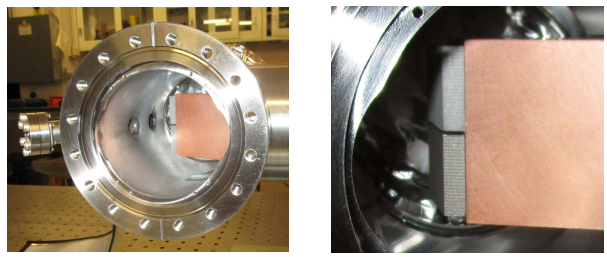

(a) Inboard view. (b) Outboard view, zoomed.

Figure 1: Upstream views of the Cu scraper and mounted Al- and Ti-alloy collimator test pieces.

A significant simulation effort was undertaken to support the collimator irradiation studies using `elegant` [5] and its parallellized version `Pelegant` [6–8]. Simulation details are provided in a companion paper [9] at this conference.

EXPERIMENT

Studies were conducted May 18-19, 2019 at a beam energy of 6 GeV. The scraper/collimator assembly was installed in the Sector 37 (S37) straight section. One of the goals called for increasing beam current up to 150 mA to more closely match the on-target dose expected in APS-U.

Study Setup

The aluminum and titanium alloy collimators were mounted on a calibrated, LVDT-actuated scraper for horizontal insertion into the beam chamber. Temperature and pressure readings were closely monitored during the study. Along with the regular suite of diagnostics including BPMs, current monitors, and pinhole emittance monitor, a camera system was installed to look directly at the beam-facing collimator surface before, during, and after beam irradiation. Fast beam loss monitors (BLMs) were also employed to observe the temporal evolution of the dump process.

Prior to the planned beam dumps, an experiment was conducted to accurately measure the location of the 1-mm gap between the collimator pieces (see Fig. 1b). This was done at low-current (~2 mA) by first moving the scraper such that the collimator surface was within a few millimeters of the beam, horizontally. The beam was then scanned vertically. Due to variations in horizontal acceptance, the beam lifetime (LT) is reduced as the beam approaches the vacuum chamber

* Work supported by the U.S. Department of Energy, Office of Science, Office of Basic Energy Sciences, under Contract No. DE-AC02-06CH11357.
† jcdooling@anl.gov

ISBN: 978-3-95450-223-3 ISSN: 2673-7000 doi:10.18429/JACoW-NAPAC2019-MOPLM14

wall; thus near the gap, LT will increase. The location where LT peaked was identified as the center of the gap and designated as y=0 for the orbit bumps. A `Pelegant` simulation of this experiment is compared with the measured LT scan data in Fig. 2.

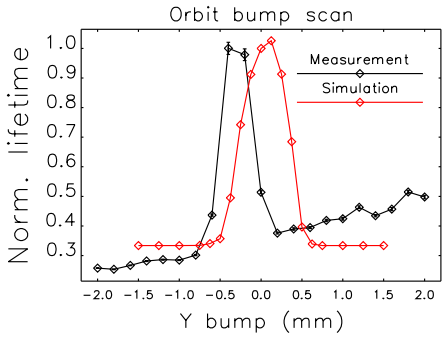

Figure 2: Beam lifetime during vertical scan near collimator surface to identify the gap between the materials.

Beam Dumps

Due to unrelated operations issues, the beam current was limited to less than 70 mA. Data were collected for a reduced set of conditions given in Table 1. For the lower current cases,

Table 1: S37 Collimator Beam Dump Cases

Case	I_b (mA)	y-offset (mm)	No. bunches*	Mat'l	charge/ bunch (nC)
0	1.8	1.80	4d	Al	1.66
1	3.9	2.31	8d	Al	1.79
2	5.5	2.82	12d	Al	1.69
3	10.0	3.32	16d	Al	2.30
4	17.1	3.83	27s	Al	2.33
5	33.1	4.33	54s	Al	2.26
6	67.4	4.84	108s	Al	2.30
7	2.4	-1.23	4d	TiA	2.21
8	4.2	-1.74	8d	TiA	1.93
9	7.0	-2.24	12d	TiA	2.15
10	9.7	-2.75	16d	TiA	2.23
11	15.9	-3.26	27s	TiA	2.17
12	32.1	-3.76	54s	TiA	2.19
13	66.9	-0.73	108s	TiA	2.28
14	64.1	1.24	108s	Al	2.18

*d=doublet, s=singlet

charge was injected into doublets, i.e., charge was injected into symmetric groups of adjacent 352-MHz rf buckets. This improves performance of the BPMs when the total current in the SR is low. Otherwise, symmetric singlet bunches are employed.

Table 2 compares beam sizes (σ) and current densities (j_b) for the higher current cases. Significant variation in vertical emittance (ϵ_y) values are observed; whereas, horizontal emittances show little change. ϵ_x ranges from 1.794 to 1.895 nm. Of note, ϵ_y varies by 53% for the two highest current beam dumps in Al and thus current densities for the two cases nominally differ by 24%. An even greater difference is seen between the 32- and 64-mA cases on TiA, where the vertical emittance is seen to increase by almost a factor of 5 for the higher current. In this circumstance, the current densities for the 32- and 64-mA beam dumps are roughly similar, but the vertical beam size more than doubles in the higher current case.

Table 2: Beam Size and Current Density during Singlet Bunch Beam Aborts

Mat'l/ Case	I_b (mA)	ϵ_y (pm)	σ_x (μm)	σ_y (μm)	j_b (A-mm^{-2})
Al/04	17.1	8.2	104.7	7.0	3.71
Al/05	33.1	10.1	104.2	7.8	6.48
Al/06	67.4	14.7	105.2	9.4	10.85
TiA/11	15.9	4.54	104.8	5.2	4.64
TiA/12	32.1	4.98	104.4	5.5	8.90
TiA/13	66.9	24.3	104.2	12.1	8.45
Al/14	64.1	9.58	103.2	7.6	13.00

Fast Beam Loss Monitors

The variation of beam arrival time on the collimator with current is plotted in Fig. 3a. Time is measured relative to the machine protection system trigger which initiates the beam dump by muting the rf and is determined from the center of the loss distribution. Loss pulse duration for signals

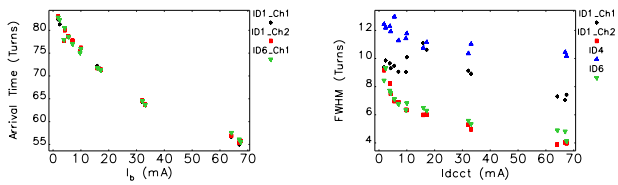

(a) Bunch Arrival Time. (b) Loss signal pulse duration.

Figure 3: a) Arrival time and b) loss duration recorded in ID1, 4, and 6.

from ID1, 4, and 6 BLMs are compared in Fig. 3b. Pulse durations seen at ID1 and ID6 are less than those observed at ID4; this is probably due to aperturing of the shower before reaching these locations. Loss pulses at ID4 have the longest duration likely due to the ID vacuum chamber there having the smallest aperture in the SR.

Diagnostic Camera

Some of the most dramatic data came in the form of images acquired with the diagnostic camera system. As seen in Fig. 4a, the camera and remote-controlled lens are mounted on the middle deck of the stand and shielded with 2-in.-thick

ISBN: 978-3-95450-223-3 ISSN: 2673-7000 doi:10.18429/JACoW-NAPAC2019-MOPLM14

(50.8 mm) Pb bricks; an optical transport line allows the camera and lens to be away from the highest radiation levels found at beam elevation. The positions of the camera and

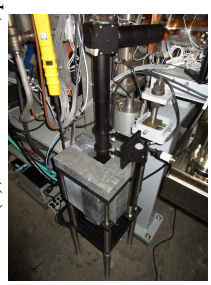

(a) Camera Stand.

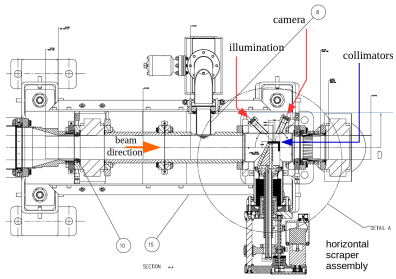

(b) Plan View Scraper/Camera.

Figure 4: a) Diagnostic camera and b) S37 scraper plan view indicating camera and illumination ports.

illumination ports relative to the scraper and collimators are shown in Fig. 4b with the scraper fully extended.

For the final two beam dumps (Cases 13 and 14), the iris of the diagnostic camera lens was reduced until the synchrotron light from the stored beam was just visible on the monitor. To obtain a better field-of-view and improved beam quality, the vertical position of the beam was moved into a region of the collimator not struck by earlier dumps. The actual beam current for Case 13 was 66.9 mA; its DVR image is presented in Fig. 5a. A similar loss was made on the aluminum piece,

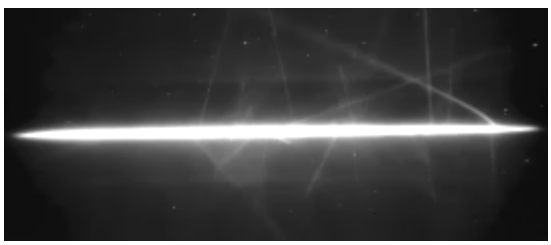

(a) Case 13, 66.9 mA on TiA.

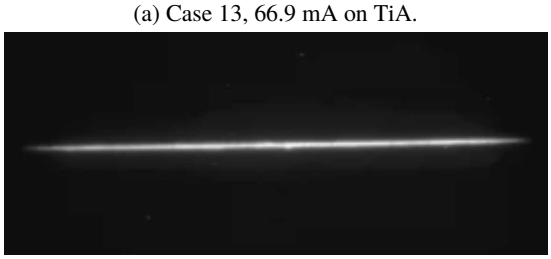

(b) Case 14, 64.1 mA on Al.

Figure 5: Diagnostic camera images of the highest current beam dumps during the May 2019 study.

also in a region previously not struck by the beam; this was the last beam dump of the study (Case 14). The DVR image for the last beam dump on Al is shown in Fig. 5b. The lens settings are identical for both cases. The light intensity for the strike on Al is significantly less than from that on TiA; in addition, no linear features are seen radiating from the Al strike region.

POST-STUDY ANALYSIS, MICROSCOPY

Comparison of 64-mA beam dump cases in Al and TiA are presented in Fig. 6. We note the appearance of a double

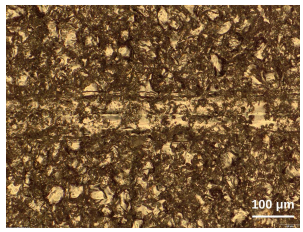

(a) Aluminum

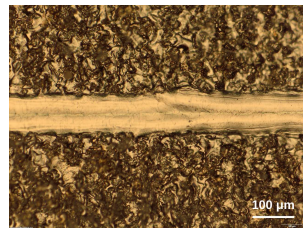

(b) Titanium Alloy.

Figure 6: Microscopy images of 64-mA beam dumps.

ridge in the region of the beam strike. The ridge pattern is more pronounced in the TiA cases; especially interesting is the much stronger modification in the surface appearance of the TiA relative to aluminum. This modification in the TiA occurs down to 16 mA, the lowest current where beam effects were observed.

DISCUSSION AND CONCLUSIONS

Both Al and Ti have naturally occurring oxide layers. The oxide layer in the beam-heated region of the aluminum collimator remains largely intact; whereas, for the TiA collimator the oxide layer is removed or absorbed. These oxide layers may act as crude thermometers; the melting temperatures of aluminum oxide (Al_2O_3) and titanium oxide (TiO_2) are 2345 K and 2116 K. One could assume based on microscopy that the irradiated region in the TiA material exceed the surface oxide's melting temperature, whereas for Al at the same current it did not. Hydrodynamic effects are visible in both materials, more so in the case of TiA.

Metallurgical analysis is ongoing; this is complicated by the fact that the TiA piece is activated. This experiment demonstrated that both Al and TiA will be damaged by APS-U whole beam dumps. In future experiments, we may evaluate advanced materials such as Molybdenum carbide-graphite [10]. Modeling with coupled hydrodynamic, particle-matter-interaction, and beam-dynamics codes is being pursued. Alternate concepts such as solid Xenon collimators are under investigation [11]. The present baseline plan for APS-U is to accept that the whole beam dump collimator is sacrificial and step the beam-facing surface after each whole beam dump event.

ACKNOWLEDGMENTS

We are indebted to the hard work of Machine Operations and Maintenance Group personnel R. Bechtold and J. Zientek for successfully leading the installation and removal of the scraper/collimator experiment. Also, thanks to R. Soliday, H. Shang, J. Stevens, S. Shoaf, R. DiViero, S. Wesling, and J. Vacca.

ISBN: 978-3-95450-223-3 ISSN: 2673-7000 doi:10.18429/JACoW-NAPAC2019-MOPLM14

REFERENCES

[1] D. Einfeld and M. Plesko, "A modified QBA optics for low emittance storage rings," *Nucl. Instrum. Methods A*, vol. 335, pp. 402–416, 1993.

[2] M. Borland *et al.*, "The Upgrade of the Advanced Photon Source," in *Proc. IPAC'18*, pp. 2872–2877, 2018.

[3] M. Borland, J. Dooling, R. Lindberg, V. Sajaev, and A. Xiao, "Using decoherence to prevent damage to the swap-out dump for the APS Upgrade," in *Proc. IPAC'18*, pp. 1494–1497, 2018.

[4] J. C. Dooling, M. Borland, Y. C. Chae, and R. Lindberg, "Energy deposition in the Sector 37 scraper of the Advanced Photon Source Storage ring," in *PAC'13*, pp. 1361–1363, 2014.

[5] M. Borland, "elegant: A Flexible SDDS-Compliant Code for Accelerator Simulation," Tech. Rep. ANL/APS LS-287, Advanced Photon Source, September 2000.

[6] Y. Wang and M. Borland, "Pelegant: A Parallel Accelerator Simulation Code for Electron Generation and Tracking," *AIP Conf. Proc.*, vol. 877, p. 241, 2006.

[7] Y. Wang, M. Borland, H. Shang, and R. Soliday, "Recent progress on parallel elegant," in *Proc. ICAP'09*, pp. 355–357, 2009.

[8] M. Borland, T. Berenc, L. Emery, and R. Lindberg, "Simultaneous simulation of multi-particle and multi-bunch collective effects for the APS ultra-low emittance upgrade," in *Proc. ICAP'15*, pp. 61–65, 2015.

[9] M. Borland *et al.*, "Simulation of Beam Aborts for the Advanced Photon Source to Probe Material-Damage Limits for Future Storage Rings," presented at NAPAC'19, MOPLM07, 2019.

[10] J. Guardia-Valenzuela *et al.*, "Development and properties of high thermal conductivity molybdenum carbide - graphite composites," *Carbon*, vol. 135, pp. 72–84, 2018.

[11] M. Borland, H. Cease, and J. C. Dooling, "Use of solid xenon as a beam dump material for 4th-generation storage rings," presented at NAPAC'19, THYBA3, 2019.